Proximity-induced nonlinear magnetoresistances on topological insulators

M. Mehraeen ⬤* and Steven S.-L. Zhang ⬤†

Department of Physics, Case Western Reserve University, Cleveland, Ohio 44106, USA

We employ quadratic-response Kubo formulas to investigate the nonlinear magnetotransport in bilayers composed of a topological insulator and a magnetic insulator, and predict both unidirectional magnetoresistance and nonlinear planar Hall effects driven by interfacial disorder and spin-orbit scattering. These effects exhibit strong dependencies on the Fermi energy relative to the strength of the exchange interaction between the spins of Dirac electrons and the interfacial magnetization. In particular, as the Fermi energy becomes comparable to the exchange energy, the nonlinear magnetotransport coefficients can be greatly amplified and their dependencies on the magnetization orientation deviate significantly from conventional sinusoidal behavior. These findings may not only deepen our understanding of the origin of nonlinear magnetotransport in magnetic topological systems but also open new pathways to probe the Fermi and exchange energies via transport measurements.

I. INTRODUCTION

Topological-insulator (TI)-based magnetic heterostructures are appealing systems for exploring the interplay between magnetism and band topology. These hybrid systems are characterized by the coexistence of strong spin-orbit coupling (SOC), sizable magnetic exchange interaction, and Dirac surface states with spin-momentum locking. Moreover, it has been demonstrated that the Fermi level of the TI layer in these systems can be finely tuned with respect to the Dirac point [1–4]. These properties are remarkable in their own rights, and a blend of them makes these systems even more intriguing. A multitude of linear-response transport phenomena have attracted considerable attention, including quantum anomalous Hall [5–10], topological Hall [11–13], spin-transfer torque [14–16], and various novel magnetoresistance effects [17–19], which may potentially lead to applications in many areas, ranging from classical information storage and processing [20] to quantum computation [21,22].

Going beyond linear responses, TI-based magnetic heterostructures also allow magnetotransport that violates Onsager's reciprocity in principle, owing to the lack of both time-reversal and inversion symmetries. Corrections to linear magnetoconductivities have been observed in a few TI-based magnetic heterostructures [23–28]—ensuing the discovery of unidirectional magnetoresistance (UMR) effects in metallic and semiconducting magnetic bilayers [29,30]. Such nonlinear magnetoconductivities are odd under the reversal of either the direction of the applied electric field **E** or that of the magnetization (whose direction will be denoted by a unit vector **m** hereafter); i.e., $\sigma^{(2)}(-\mathbf{m}, \mathbf{E}) = \sigma^{(2)}(\mathbf{m}, -\mathbf{E}) = -\sigma^{(2)}(\mathbf{m}, \mathbf{E})$,

which are distinctly different from their linear-response counterparts and hence hold fascinating prospects for adding new functionalities in future spintronic devices.

To date, studies of nonlinear transport in magnetic layered structures have mainly been focused on controlling the corresponding magnetotransport coefficients by varying the magnetization vector with an external magnetic field. And, more specifically, the reported dependencies of the nonlinear current on the magnetization direction can be cast into the simple form [28–46]

$$\mathbf{j}_1^{(2)} = \sigma_{\parallel,1}^{(2)}\mathbf{m} \cdot (\mathbf{z} \times \mathbf{E})\mathbf{E} + \sigma_{\perp,1}^{(2)}(\mathbf{m} \cdot \mathbf{E})\mathbf{z} \times \mathbf{E}, \quad (1)$$

where the unit vector **z** denotes the interface normal, and $\sigma_{\parallel,1}^{(2)}$ ($\sigma_{\perp,1}^{(2)}$) is a transport coefficient that characterizes the strength of the nonlinear current longitudinal (transverse) to the applied electric field, which is denoted by $\mathbf{j}_{\parallel,1}^{(2)}$ ($\mathbf{j}_{\perp,1}^{(2)}$). Here, the superscript 2 and the subscript 1 indicate that the nonlinear current is of second order in the applied electric field and first order in the magnetization. The tunability of these nonlinear transport coefficients upon the shift of the Fermi level, however, has remained unexplored.

In this work, we theoretically investigate nonlinear magnetotransport in magnetic bilayers consisting of a TI and a ferromagnetic-insulator (FI) layer, as shown schematically in Fig. 1. A formal evaluation of Kubo formulas in the quadratic-response regime is performed to explore the magnetoconductivities of interest. Within this quantum approach, we find a UMR effect and a nonlinear planar Hall effect (NPHE) that are driven purely by extrinsic spin-orbit scattering at the interface. More interestingly, perhaps, unconventional dependencies of the nonlinear currents on the magnetization orientation emerge, which differ from those given by Eq. (1) and feature terms that are of higher order in the magnetization. Following a symmetry analysis of the nonlinear response

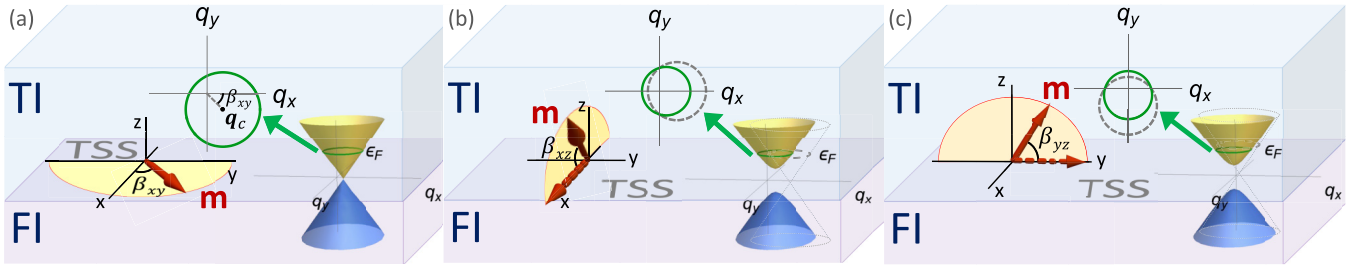*mxm1289@case.edu

†shulei.zhang@case.edu

FIG. 1. Schematics of the TI/FI bilayer system and the topological surface state (TSS). (a) In-plane rotation of the magnetization, which leads to a rigid shift of the Dirac cone and thus the Fermi contour. (b) and (c) Out-of-plane rotations of the magnetization, which gap the system. In this case, in addition to a shift, the radius of the Fermi contour is decreased as the magnetization is rotated out of the bilayer plane. Here, β_{ij} ($i, j = x, y, z$) is the angle between the i axis and the magnetization as it sweeps the ij plane.

function, the details of which are presented in Appendix A, the general nonlinear current may be expressed as

$$\mathbf{j}_\parallel^{(2)} = \mathbf{j}_{\parallel,1}^{(2)}[1+\iota_\parallel(\mathbf{m}\cdot\mathbf{e})^2+\kappa_\parallel(\mathbf{m}\cdot\mathbf{z}\times\mathbf{e})^2+\lambda_\parallel(\mathbf{m}\cdot\mathbf{z})^2],$$
(2a)

$$\mathbf{j}_\perp^{(2)} = \mathbf{j}_{\perp,1}^{(2)}[+\iota_\perp(\mathbf{m}\cdot\mathbf{e})^2+\kappa_\perp(\mathbf{m}\cdot\mathbf{z}\times\mathbf{e})^2+\lambda_\perp(\mathbf{m}\cdot\mathbf{z})^2],$$
(2b)

where $\mathbf{e}$ is the unit vector along the electric field. Here, $\iota_{\parallel,\perp}$, $\kappa_{\parallel,\perp}$ and $\lambda_{\parallel,\perp}$ are dimensionless quantities that characterize the strengths of the contributions cubic in the magnetization and are, in general, functions of disorder and the exchange energy. Intriguingly, when the Fermi and exchange energies become comparable, the nonlinear magnetoresistances may be considerably amplified and the contributions of the cubic terms become relatively large, leading to strong deviations in the angular dependencies. These new features may then be used to obtain insights about the position of the Fermi level or the strength of the interfacial exchange interaction via transport measurements, as a simple alternative to optical schemes such as ARPES.

II. DISORDER SCATTERING IN TI SURFACE STATES

Let us commence with a minimal model for the surface states on a TI adjacent to a FI layer, which may be expressed as

$$\hat{H}_{\mathbf{qq}'} = \hat{H}_\mathbf{q}^0\delta_{\mathbf{qq}'} + \hat{V}_{\mathbf{qq}'},$$
(3a)

$$\hat{H}_\mathbf{q}^0 = \hat{\boldsymbol{\sigma}}\cdot\mathbf{h_q} + \Delta_{\text{ex}}\hat{\sigma}_z m_z,$$
(3b)

where $\mathbf{h_q} = \hbar v_F\mathbf{q}\times\mathbf{z} - \Delta_{\text{ex}}\mathbf{z}\times(\mathbf{z}\times\mathbf{m})$, with $\mathbf{q}$ the in-plane momentum, v_F the Fermi velocity, Δ_{ex} the proximity-induced exchange energy, and $\mathbf{m} = (m_x, m_y, m_z)$ the unit magnetization. For the impurity potential $\hat{V}_{\mathbf{qq}'}$, we assume it consists of contributions from scalar point scatterers, $\hat{U}_{\mathbf{qq}'}$, as well as from the SOC of the random structural defects [47], $\hat{W}_{\mathbf{qq}'}$, as [48–53]

$$\hat{V}_{\mathbf{qq}'} = \hat{U}_{\mathbf{qq}'} + \hat{W}_{\mathbf{qq}'},$$
(4a)

$$\hat{U}_{\mathbf{qq}'} = U_{\mathbf{qq}'}^0\hat{\sigma}_0,$$
(4b)

$$\hat{W}_{\mathbf{qq}'} = \tfrac{1}{2}W_{\mathbf{qq}'}^0\hat{\boldsymbol{\sigma}}\cdot(\mathbf{q}+\mathbf{q}')\times\mathbf{z}.$$
(4c)

And we assume the white noise distribution for the disorder potentials, $\langle U_{\mathbf{qq}'}^0\rangle = 0$, $\langle U_{\mathbf{qq}'}^0 U_{\mathbf{q'q}}^0\rangle = n_I U_0^2$, $\langle W_{\mathbf{qq}'}^0\rangle = 0$,

and $\langle W_{\mathbf{qq}'}^0 W_{\mathbf{q'q}}^0\rangle = n_\alpha W_0^2$, where $\langle\cdots\rangle$ denotes the impurity average, and n_I and n_α are the densities of the scalar and SOC scatterers, while U_0 and W_0 measure the strengths of the disorder interactions.

III. SCATTERING TIME AND QUADRATIC RESPONSE

In this section, the nonlinear magnetotransport coefficients in the system under consideration are examined by evaluating quadratic Kubo formulas, which–diagrammatically— correspond to triangle diagrams of response theory [54–57], as shown in Fig. 2. This is an essential diagrammatic approach, as UMRs and nonlinear Hall effects cannot be captured by the two-photon bubble diagrams of linear response theory.

The self-energy in the Born approximation is given by

$$\Sigma_{\mathbf{q}\sigma}^{\text{R/A}}(\epsilon) = \sum_{\mathbf{q}'\sigma'}\langle V_{\mathbf{qq}'}^{\sigma\sigma'}V_{\mathbf{q'q}}^{\sigma'\sigma}\rangle G_{\mathbf{q}'\sigma'}^{0,\text{R/A}}(\epsilon),$$
(5)

where $\sum_\mathbf{q}\equiv\int d^2\mathbf{q}/(2\pi)^2$ and $G_{\mathbf{q}\sigma}^{0,\text{R/A}}(\epsilon) = (\epsilon - \epsilon_{\mathbf{q}\sigma} \pm i\delta)^{-1}$ is the retarded/advanced Green's function of the unperturbed system $\hat{H}_\mathbf{q}^0$, with the eigenvalue $\epsilon_{\mathbf{q}\sigma} = \sigma\sqrt{h_\mathbf{q}^2 + \Delta_{\text{ex}}^2 m_z^2}$ for the band σ ($= \pm$). The scattering time is given by $\tau_{\mathbf{q}\sigma}(\epsilon) = \hbar/2\Gamma_{\mathbf{q}\sigma}(\epsilon)$, with the scattering rate defined as $\Gamma_{\mathbf{q}\sigma} \equiv -\text{Im}\Sigma_{\mathbf{q}\sigma}^\text{R}$. Upon introducing the change of variables $\eta_\mathbf{h} \equiv \mathbf{h_q}/\epsilon$ and $\eta_\text{ex} \equiv \Delta_\text{ex}/\epsilon$, as detailed in Appendix B,
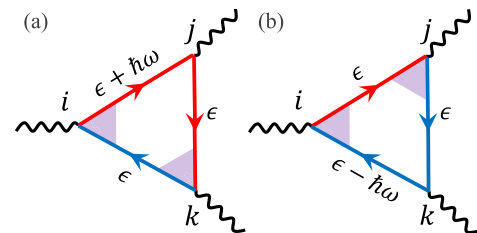

FIG. 2. Diagrammatic structure of the quadratic response. Panels (a) and (b), along with their $j \leftrightarrow k$ counterparts, are the four triangle diagrams that give rise to the UMR and NPHE. The red (blue) arrowed lines represent retarded (advanced) dressed electron Green's functions, while purple shaded areas indicate dressed vertices. The vertices are labeled by the spatial index of their external photons, while propagators are labeled by their energies.

we find

$$\tau_{\mathbf{q}\sigma} = \frac{\hbar}{2\Gamma_I}\left[1 + \sigma\eta_{\mathrm{ex}}m_z\cos\theta_{\mathbf{h}} + \frac{\Gamma_\alpha}{\Gamma_I}\mathcal{F}_\sigma(\boldsymbol{\eta}_{\mathbf{h}}, \eta_{\mathrm{ex}}; \mathbf{m})\right]^{-1},$$

(6)

where $\Gamma_I \equiv n_I U_0^2\epsilon/(2\hbar v_F)^2$ and $\Gamma_\alpha \equiv n_\alpha W_0^2\epsilon^3/(2\hbar v_F)^4$ are the scalar and SOC disorder self-energy coefficients, respectively, and $\theta_{\mathbf{h}} = \cos^{-1}(\eta_{\mathrm{ex}}m_z/\sqrt{\eta_{\mathbf{h}}^2 + \eta_{\mathrm{ex}}^2 m_z^2})$. The dimensionless band-dependent function $\mathcal{F}_\sigma$—whose explicit form is presented in Appendix B—is a rather complicated function of the Fermi velocity, exchange energy, and orientation of the magnetization. As we discuss below, this nontrivial angular dependence of the scattering time on the magnetization direction plays an important role in explaining the unconventional angular dependencies of the nonlinear magnetoresistances.

The quadratic conductivity tensor is obtained by evaluating the four triangle diagrams shown in Fig. 2. Together, their contributions to the nonlinear dc conductivity may be succinctly expressed as [56]

$$\sigma^{ijk} = \frac{e^3\hbar^2}{\pi}\mathrm{Im}\sum_{\mathbf{q}\sigma}\partial_\omega\left[\mathcal{V}_{\mathbf{q}\sigma}^i(\epsilon_F, \epsilon_F + \hbar\omega)G_{\mathbf{q}\sigma}^R(\epsilon_F + \hbar\omega)\right]_{\omega=0}$$

$$\times\, v_{\mathbf{q}\sigma}^j G_{\mathbf{q}\sigma}^R(\epsilon_F)\mathcal{V}_{\mathbf{q}\sigma}^{kF}G_{\mathbf{q}\sigma}^A(\epsilon_F) + (j\leftrightarrow k).$$

(7)

Here ϵ_F is the Fermi energy and $G_{\mathbf{q}\sigma}^{R/A}(\epsilon) = (\epsilon - \epsilon_{\mathbf{q}\sigma} \pm i\Gamma_{\mathbf{q}\sigma})^{-1}$ is the disorder-dressed electron Green's function. The (bare) velocity operator is defined as $\hat{\mathbf{v}}_{\mathbf{q}} = \partial_{\mathbf{q}}\hat{H}_{\mathbf{q}}^0/\hbar$, with $\partial_{\mathbf{q}}^i \equiv \partial/\partial q_i$, which—in the chiral basis of Bloch eigenstates—leads to the diagonal terms $\mathbf{v}_{\mathbf{q}\sigma} = \partial_{\mathbf{q}}\epsilon_{\mathbf{q}\sigma}/\hbar$. $\mathcal{V}_{\mathbf{q}\sigma}(\epsilon, \epsilon')$, which is presented in Appendix C, is the disorder-averaged velocity vertex function, where ϵ and ϵ' are, respectively, the energies of the incoming and outgoing propagators to the vertex in question and $\mathcal{V}_{\mathbf{q}\sigma}^F \equiv \mathcal{V}_{\mathbf{q}\sigma}(\epsilon_F, \epsilon_F)$.

IV. ANGULAR DEPENDENCIES

Without loss of generality, let us set the electric field along the x direction, $\mathbf{e} = \mathbf{x}$. Then it suffices to calculate the σ_{xxx} and σ_{yxx} elements of the conductivity tensor. To characterize the nonlinear transport, we introduce the longitudinal and transverse UMR coefficients $\zeta_\parallel^{(2)} = \zeta_x^{(2)}$ and $\zeta_\perp^{(2)} = \zeta_y^{(2)}$, where

$$\zeta_i^{(2)} \equiv \frac{\sigma_{ix}(E_x) - \sigma_{ix}(-E_x)}{\sigma_D E_x} \simeq -\frac{2\sigma_{ixx}}{\sigma_D}$$

(8)

to leading order in the electric field. Here $\sigma_{ij} = j_i/E_j$ denotes the linear conductivity tensor and $\sigma_D = e^2/[4\pi\hbar(\eta_I + \eta_\alpha)]$ is the Drude conductivity, with $\eta_I \equiv \Gamma_I/\epsilon_F$ and $\eta_\alpha \equiv \Gamma_\alpha/\epsilon_F$ the dimensionless disorder coefficients.

Plots of the UMR coefficients for various angular sweeps of the magnetization are presented in Fig. 3. As shown by the blue curves in Figs. 3(a) and 3(b), we see that as the Fermi level approaches the exchange energy, i.e., when η_{ex} is closer to one, the strength of the longitudinal nonlinear magnetoresistance $\zeta_\parallel^{(2)}$ is significantly amplified and can be as large as one to two orders of magnitude stronger than when η_{ex} is smaller (see the dashed green and dotted pink curves). Furthermore, qualitatively, the angular dependencies of the longitudinal UMR coefficient increasingly deviate from the conventional sinusoidal behavior as η_{ex} is increased.
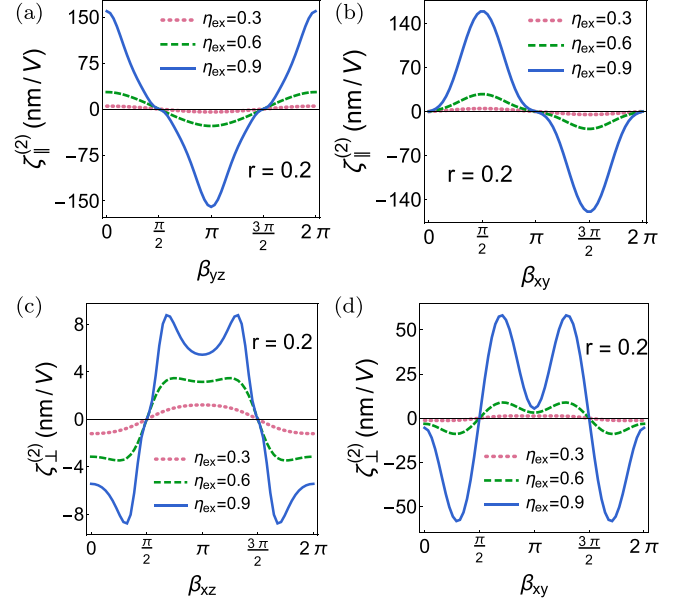

FIG. 3. Angular dependencies of the UMR coefficients as the magnetization direction is varied in the xy, yz, and xz planes (the xz scan for $\zeta_\parallel^{(2)}$ and yz scan for $\zeta_\perp^{(2)}$ vanish due to symmetry constraints and hence are not shown here). Parameters used: $\epsilon_F = 0.5$ eV, $v_F = 5\times10^{14}$ nm/s [58], and $\eta_I = 0.01$.

Quantitatively, the situation is similar for the NPHE; as shown by the blue curves in Figs 3(c) and 3(d), the transverse UMR coefficient $\zeta_\perp^{(2)}$ is larger when the Fermi level is closer to the exchange energy. Qualitatively, however, as η_{ex} is increased, the NPHE no longer reaches its maximal absolute value at the expected angles $\beta_{xz}, \beta_{xy} = 0, \pi$ (see the pink curves), which is when the magnetization is entirely along the x axis; instead, there is an emergent bifurcation of the peaks and troughs such that the maximal absolute values of the NPHE are obtained when the magnetization is only partially along the x axis [59].

Further analysis reveals that the angular profiles of both the UMR and NPHE are also sensitive to the ratio of the scalar to SOC disorder present in the system, $r \equiv \eta_I/\eta_\alpha$ (see Appendix D for details). To capture the angular dependencies of the nonlinear responses, combining Eqs. (2) and (8), the corresponding UMR coefficients with the magnetization direction being varied in the three orthogonal planes are expressed as

$$\zeta_\parallel^{(2)}\big|_{m_x=0} \simeq f_\parallel(\eta_{\mathrm{ex}}, r)\cos\beta_{yz} + g_\parallel(\eta_{\mathrm{ex}}, r)\cos^3\beta_{yz},$$ (9a)

$$\zeta_\perp^{(2)}\big|_{m_y=0} \simeq f_\perp(\eta_{\mathrm{ex}}, r)\cos\beta_{xz} + g_\perp(\eta_{\mathrm{ex}}, r)\cos^3\beta_{xz}$$ (9b)

for the out-of-plane sweeps of the magnetization and

$$\zeta_\parallel^{(2)}\big|_{m_z=0} \simeq h_\parallel(\eta_{\mathrm{ex}}, r)\sin\beta_{xy} + k_\parallel(\eta_{\mathrm{ex}}, r)\sin^3\beta_{xy},$$ (10a)

$$\zeta_\perp^{(2)}\big|_{m_z=0} \simeq h_\perp(\eta_{\mathrm{ex}}, r)\cos\beta_{xy} + k_\perp(\eta_{\mathrm{ex}}, r)\cos^3\beta_{xy}$$ (10b)

for the in-plane sweep, where the functions on the right-hand side—which, in general, depend on η_{ex} and r—are given by

$$f_\parallel(\eta_{\mathrm{ex}}, r) = -\frac{2\sigma_{\parallel,1}^{(2)}}{\sigma_D}(1 + \lambda_\parallel),$$

(11a)

TABLE I. Transport coefficients for the cubic contributions to the UMR and NPHE at $r = 0.2$ and for different values of η_{ex}. For the rest of the parameters used, see the caption of Fig. 3.

η_{ex}	$a_{\parallel}$	$b_{\parallel}$	$a_{\perp}$	$b_{\perp}$
0.3	0.03	0.30	-0.20	-0.47
0.6	0.09	1.92	-0.59	-0.85

$$g_{\parallel}(\eta_{\text{ex}}, r) = -\frac{2\sigma_{\parallel,1}^{(2)}}{\sigma_D}(\kappa_{\parallel} - \lambda_{\parallel}), \tag{11b}$$

$$h_{\parallel}(\eta_{\text{ex}}, r) = -\frac{2\sigma_{\parallel,1}^{(2)}}{\sigma_D}(1 + \iota_{\parallel}), \tag{11c}$$

$$k_{\parallel}(\eta_{\text{ex}}, r) = -\frac{2\sigma_{\parallel,1}^{(2)}}{\sigma_D}(\kappa_{\parallel} - \iota_{\parallel}), \tag{11d}$$

and

$$f_{\perp}(\eta_{\text{ex}}, r) = -\frac{2\sigma_{\perp,1}^{(2)}}{\sigma_D}(1 + \lambda_{\perp}), \tag{12a}$$

$$g_{\perp}(\eta_{\text{ex}}, r) = -\frac{2\sigma_{\perp,1}^{(2)}}{\sigma_D}(\iota_{\perp} - \lambda_{\perp}), \tag{12b}$$

$$h_{\perp}(\eta_{\text{ex}}, r) = -\frac{2\sigma_{\perp,1}^{(2)}}{\sigma_D}(1 + \kappa_{\perp}), \tag{12c}$$

$$k_{\perp}(\eta_{\text{ex}}, r) = -\frac{2\sigma_{\perp,1}^{(2)}}{\sigma_D}(\iota_{\perp} - \kappa_{\perp}). \tag{12d}$$

To quantify the deviations of the UMR coefficients from sinusoidal behavior for various sweeps of the magnetization, we introduce the dimensionless ratios $a_{\parallel} \equiv g_{\parallel}/f_{\parallel}$, $b_{\parallel} \equiv k_{\parallel}/h_{\parallel}$, $a_{\perp} \equiv g_{\perp}/f_{\perp}$, and $b_{\perp} \equiv k_{\perp}/h_{\perp}$. The values of these ratios for $\eta_{\text{ex}} = 0.3$ and $\eta_{\text{ex}} = 0.6$ are presented in Table I, from which it is evident that the cubic terms play an increasingly important—and even dominant—role as the exchange and Fermi energies become comparable. It is worth mentioning that for even higher values of η_{ex}, as indicated by the blue curves in Fig. 3, the UMR coefficients become increasingly nonlinear in the magnetization, such that higher-order terms in the magnetization must also be taken into account.

V. DISCUSSION AND CONCLUSION

In order to understand the physical origin of the unconventional angular dependencies of the UMR and NPHE, we note that this occurs for larger values of η_{ex}. In systems where the Fermi energy is fixed, it often suffices to consider terms only to first order in the magnetization, which typically leads to sinusoidal angular dependencies. In TIs, however, the tunability of the Fermi level implies that higher-order terms in the magnetization are expected to play an important role when $\eta_{\text{ex}} \sim 1$, thereby necessitating the cubic magnetization terms in Eq. (2).

This is in contrast to nonlinear magnetotransport phenomena driven by hexagonal warping or particle-hole asymmetry [60,61]. In the case of warping, the sixfold symmetric

deformation of the Fermi contour arises from the addition of a cubic-in-momentum term to the Dirac Hamiltonian, while particle-hole asymmetry adds a k^2 term to the Hamiltonian. Thus, both effects are dominant in the limit of high Fermi energy, i.e., when $\eta_{\text{ex}} \ll 1$, thereby enabling a simple way to distinguish their contributions from the ones presented in this work.

Another nonlinear transport effect which is stronger in the low Fermi energy limit is that generated by current-induced spin polarization. However, the contribution of this effect to the nonlinear transport can be distinguished from the mechanism predicted here by noting that current-induced spin polarization can only produce a longitudinal quadratic response with no quadratic planar Hall counterpart. This may readily be understood by noting that the emergence of a NPHE requires the magnetization to be parallel to the applied current, which, in turn, is perpendicular to the spin polarization. As a result, the magnetization cannot influence the spin polarization and no quadratic Hall response is generated [23,52,62,63].

In addition, in terms of magnitude, the UMR coefficient strengths that we predict here are on the order of 10–100 nm/V and are thus one to two orders of magnitude larger than the bilinear magnetoresistance effect predicted in non-magnetic TIs [52]. This can be attributed to the fact the proximity-induced exchange interaction is much stronger than the Zeeman interaction for typical experimental magnetic field values, and suggests that TI/FI bilayers are generally a better platform for obtaining sizable nonlinear magnetotransport effects.

Yet another quadratic transport effect that can arise in TI/FI bilayers is the intrinsic nonlinear Hall effect generated by the Berry curvature dipole [64]. However, this relies on an out-of-plane magnetization, in contrast to the NPHE predicted in this work, which only arises when the magnetization has an in-plane component. Furthermore, the absence of a longitudinal UMR generated by the Berry curvature dipole provides an additional means to distinguish it from the effects predicted here.

A final point worth mentioning is that the minimal model we consider here for the Dirac surface states is quite general and is not limited to TI/FI bilayer systems. Thus, it is natural to expect that the nonlinear transport effects predicted in this work should, in principle, also arise in generally magnetized TI systems, including intrinsic magnetic TIs [65,66], magnetically doped TIs [67–69], as well as in single TI layers in the presence of an applied magnetic field.

In conclusion, based on a formal evaluation of nonlinear Kubo formulas in the low-temperature limit, we have predicted a UMR and NPHE in a bilayer comprised of a TI and a FI which require no modification of the Dirac Hamiltonian, but instead arise solely from extrinsic disorder scattering at the interface. Several key features and unique transport signatures have been identified, which enable the electric and magnetic tuning of the nonlinear magnetoresistance effects. We expect that this work will stimulate further theoretical and experimental studies of quantum transport in the nonlinear response regime, paving the way for potential future quantum spintronic applications.

APPENDIX A: SYMMETRY ANALYSIS OF NONLINEAR RESPONSES

In this section, we derive the general form of the nonlinear current, $j_i^{(2)} = \sigma_{ijk} E^j E^k$, to third order in the magnetization for the TI/FI bilayer system described by Eq. (3). To this end, consider the magnetization expansion of the quadratic conductivity tensor:

$$\sigma^{ijk} = \sigma_1^{ijkl} m_l + \sigma_2^{ijklm} m_l m_m + \sigma_3^{ijklmn} m_l m_m m_n. \quad (A1)$$

Without loss of generality, let us set the electric field in the x direction so that we need only evaluate σ^{xxx} for the longitudinal current. Note that in the absence of the exchange interaction, the system is even under the mirror reflection transformation in the xz (yz) plane, $\mathcal{M}_{xz}$ ($\mathcal{M}_{yz}$), and thus so are σ_1, σ_2, and σ_3. Using the fact that the current and magnetization are polar and axial vectors, respectively, it is then straightforward to verify that, upon imposing $\mathcal{M}_{xz}$ and $\mathcal{M}_{yz}$, $\sigma_1^{xxxx} = \sigma_1^{xxxz} = 0$, while, in general, $\sigma_1^{xxxy} \neq 0$. Similarly, for the quadratic contribution, one can verify that only terms $\propto m_x m_z$ are allowed by reflection symmetry. However, given the particle-hole symmetry and the quadratic dependence of the disorder averages on m_z [see Eq. (B3)], the terms linear in m_z do not contribute to the nonlinear response, and σ_2, therefore, plays no role in the nonlinear transport.

Moving on to the cubic contribution, one can verify that, in addition to σ_3^{xxxxyz}, terms containing even powers of m_y do not contribute to $j_x^{(2)}$. Thus, of the ten independent components of σ_3^{xxxijk}, only three survive the symmetry requirements, namely σ_3^{xxxyxx}, σ_3^{xxxyyy}, and σ_3^{xxxyzz}. By an analogous argument for the transverse current, one can show that only the independent components σ_1^{yxxx}, σ_3^{yxxxxx}, σ_3^{yxxxyy}, and σ_3^{yxxxzz} may be nonvanishing. Therefore, the nonlinear current up to third order in the magnetization may be expressed as

$$j_x^{(2)} = j_{x,1}^{(2)}\left(1 + \iota_\parallel m_x^2 + \kappa_\parallel m_y^2 + \lambda_\parallel m_z^2\right), \quad (A2a)$$

$$j_y^{(2)} = j_{y,1}^{(2)}\left(1 + \iota_\perp m_x^2 + \kappa_\perp m_y^2 + \lambda_\perp m_z^2\right), \quad (A2b)$$

where $j_{x,1}^{(2)} = \sigma_1^{xxxy} m_y E_x^2$, $j_{y,1}^{(2)} = \sigma_1^{yxxx} m_x E_x^2$ and the dimensionless functions measuring the cubic contributions read

$$\iota_\parallel = \frac{3\sigma_3^{xxxyxx}}{\sigma_1^{xxxy}}, \quad (A3a)$$

$$\kappa_\parallel = \frac{\sigma_3^{xxxyyy}}{\sigma_1^{xxxy}}, \quad (A3b)$$

$$\lambda_\parallel = \frac{3\sigma_3^{xxxyzz}}{\sigma_1^{xxxy}}, \quad (A3c)$$

and

$$\iota_\perp = \frac{\sigma_3^{yxxxxx}}{\sigma_1^{yxxx}}, \quad (A4a)$$

$$\kappa_\perp = \frac{3\sigma_3^{yxxxyy}}{\sigma_1^{yxxx}}, \quad (A4b)$$

$$\lambda_\perp = \frac{3\sigma_3^{yxxxzz}}{\sigma_1^{yxxx}}. \quad (A4c)$$

Relaxing the orientation of the electric field to point in an arbitrary direction in the xy plane, we arrive at Eq. (2), where the functions ι, κ, and λ are now understood to be evaluated with the relevant tensor components in the basis spanned by $\mathbf{e}$, $\mathbf{z} \times \mathbf{e}$, and $\mathbf{z}$.

APPENDIX B: SELF-ENERGY AND SCATTERING TIME

The unperturbed Hamiltonian, Eq. (3b), has eigenstates given by

$$|u_{\mathbf{q}\sigma}\rangle = \begin{pmatrix} \left(\frac{1+\sigma}{2}\right)\cos\frac{\theta_{\mathbf{h}}}{2} + \left(\frac{1-\sigma}{2}\right)\sin\frac{\theta_{\mathbf{h}}}{2} \\ e^{i\phi_{\mathbf{h}}}\left[\left(\frac{1+\sigma}{2}\right)\sin\frac{\theta_{\mathbf{h}}}{2} - \left(\frac{1-\sigma}{2}\right)\cos\frac{\theta_{\mathbf{h}}}{2}\right] \end{pmatrix}, \quad (B1)$$

where $\phi_{\mathbf{h}}$ is the azimuthal angle in the plane spanned by $\mathbf{h}_{\mathbf{q}}$, with $\cos\phi_{\mathbf{h}} = h_{x\mathbf{q}}/h_{\mathbf{q}}$ and $\sin\phi_{\mathbf{h}} = h_{y\mathbf{q}}/h_{\mathbf{q}}$, while $\theta_{\mathbf{h}}$ is the polar angle, with $\sin\theta_{\mathbf{h}} = h_{\mathbf{q}}/\sqrt{h_{\mathbf{q}}^2 + \Delta_{\text{ex}}^2 m_z^2}$. The velocity operator is defined as $\hat{\mathbf{v}}_{\mathbf{q}} = \boldsymbol{\partial}_{\mathbf{q}}\hat{H}_{\mathbf{q}}^0/\hbar$, with $\partial_{\mathbf{q}}^i \equiv \partial/\partial q_i$, which, in the chiral basis of Bloch eigenstates, leads to the diagonal terms $\mathbf{v}_{\mathbf{q}\sigma} = \partial_{\mathbf{q}}\epsilon_{\mathbf{q}\sigma}/\hbar$, or

$$v_{\mathbf{q}\sigma}^x = -\sigma v_F \sin\theta_{\mathbf{h}} \sin\phi_{\mathbf{h}}, \quad (B2a)$$

$$v_{\mathbf{q}\sigma}^y = \sigma v_F \sin\theta_{\mathbf{h}} \cos\phi_{\mathbf{h}}. \quad (B2b)$$

In the chiral Bloch basis the disorder averages read

$$\langle V_{\mathbf{qq'}}^{\sigma\sigma'} V_{\mathbf{q'q}}^{\sigma'\sigma} \rangle = \langle U_{\mathbf{qq'}}^{\sigma\sigma'} U_{\mathbf{q'q}}^{\sigma'\sigma} \rangle + \langle W_{\mathbf{qq'}}^{\sigma\sigma'} W_{\mathbf{q'q}}^{\sigma'\sigma} \rangle, \quad (B3a)$$

$$\langle U_{\mathbf{qq'}}^{\sigma\sigma'} U_{\mathbf{q'q}}^{\sigma'\sigma} \rangle = \frac{1}{2}n_I U_0^2[1 + \sigma\sigma'\cos\theta_{\mathbf{h}}\cos\theta_{\mathbf{h'}} + \sigma\sigma'\cos(\phi_{\mathbf{h}} - \phi_{\mathbf{h'}})\sin\theta_{\mathbf{h}}\sin\theta_{\mathbf{h'}}], \quad (B3b)$$

$$\langle W_{\mathbf{qq'}}^{\sigma\sigma'} W_{\mathbf{q'q}}^{\sigma'\sigma} \rangle = \frac{1}{8}n_\alpha W_0^2\{[1 - \sigma\sigma'\cos\theta_{\mathbf{h}}\cos\theta_{\mathbf{h'}}][(q_x + q_x')^2 + (q_y + q_y')^2]$$
$$- \sigma\sigma'\cos(\phi_{\mathbf{h}} + \phi_{\mathbf{h'}})\sin\theta_{\mathbf{h}}\sin\theta_{\mathbf{h'}}[(q_x + q_x')^2 - (q_y + q_y')^2]$$
$$- 2\sigma\sigma'\sin(\phi_{\mathbf{h}} + \phi_{\mathbf{h'}})\sin\theta_{\mathbf{h}}\sin\theta_{\mathbf{h'}}(q_x + q_x')(q_y + q_y')\}, \quad (B3c)$$

where $V_{\mathbf{qq'}}^{\sigma\sigma'} \equiv \langle u_{\mathbf{q}\sigma}|\hat{V}_{\mathbf{qq'}}|u_{\mathbf{q'}\sigma'}\rangle$. Inserting Eq. (B3) into Eq. (5), we obtain

$$\Gamma_{\mathbf{q}\sigma} = \Gamma_I\left[1 + \sigma\eta_{\text{ex}}m_z\cos\theta_{\mathbf{h}} + \frac{\Gamma_\alpha}{\Gamma_I}\mathcal{F}_\sigma(\boldsymbol{\eta}_{\mathbf{h}}, \eta_{\text{ex}}; \mathbf{m})\right], \quad (B4)$$

where the dimensionless function $\mathcal{F}_\sigma$ reads

$$\mathcal{F}_\sigma(\boldsymbol{\eta_h}, \eta_{ex}; \mathbf{m}) = (1 - \sigma \eta_{ex} m_z \cos\theta_\mathbf{h})[1 + \eta_\mathbf{h}^2 + \eta_{ex}^2(4 - 5m_z^2)$$
$$- 4\eta_{ex}\boldsymbol{\eta_h} \cdot \mathbf{m}] + 2\sigma \sin\theta_\mathbf{h}(1 - \eta_{ex}^2 m_z^2)$$
$$\times \left(\boldsymbol{\eta_h} - 2\eta_{ex}\frac{\boldsymbol{\eta_h} \cdot \mathbf{m}}{\eta_\mathbf{h}}\right), \qquad (B5)$$

in which we assume the Fermi level lies in the upper band ($\epsilon > 0$). From this, we arrive at the momentum scattering time, Eq. (6).

APPENDIX C: VERTEX CORRECTION AND NONLINEAR CONDUCTIVITY

The disorder-averaged velocity vertex function may be found self-consistently from the general vertex equation

$$\boldsymbol{\mathcal{V}}_{\mathbf{q}\sigma}(\epsilon, \epsilon') = \mathbf{v}_{\mathbf{q}\sigma} + \sum_{\mathbf{q}'\sigma'} \langle V_{\mathbf{q}\mathbf{q}'}^{\sigma\sigma'} V_{\mathbf{q}'\mathbf{q}}^{\sigma'\sigma} \rangle G_{\mathbf{q}'\sigma'}^{A/R}(\epsilon)$$
$$\times \boldsymbol{\mathcal{V}}_{\mathbf{q}'\sigma'}(\epsilon, \epsilon') G_{\mathbf{q}'\sigma'}^{R/A}(\epsilon'), \qquad (C1)$$

where ϵ and ϵ' are, respectively, the energies of the incoming and outgoing Green's functions to the vertex in question. The near-dc behavior may be captured by setting $\epsilon' = \epsilon + \hbar\omega$. Then, using the identity

$$G_{\mathbf{q}\sigma}^{A/R}(\epsilon)G_{\mathbf{q}\sigma}^{R/A}(\epsilon + \hbar\omega) \simeq \frac{2\pi}{\hbar}\frac{\tau_{\mathbf{q}\sigma}}{1 \mp i\omega\tau_{\mathbf{q}\sigma}}\delta(\epsilon_{\mathbf{q}\sigma} - \epsilon), \quad (C2)$$

the vertex function may be approximated as

$$\boldsymbol{\mathcal{V}}_{\mathbf{q}\sigma}(\epsilon, \epsilon + \hbar\omega) \simeq \mathbf{v}_{\mathbf{q}\sigma} + \frac{2\pi}{\hbar}\sum_{\mathbf{q}'\sigma'}\langle V_{\mathbf{q}\mathbf{q}'}^{\sigma\sigma'} V_{\mathbf{q}'\mathbf{q}}^{\sigma'\sigma}\rangle$$
$$\times \frac{\tau_{\mathbf{q}'\sigma'}}{1 \mp i\omega\tau_{\mathbf{q}'\sigma'}}\mathbf{v}_{\mathbf{q}'\sigma'}\delta(\epsilon_{\mathbf{q}'\sigma'} - \epsilon). \quad (C3)$$

To obtain an approximate form for the conductivity tensor, we insert Eq. (C3) into Eq. (7) and use the identity

$$[G_{\mathbf{q}\sigma}^R(\epsilon)]^{m+1}[G_{\mathbf{q}\sigma}^A(\epsilon)]^{n+1} \simeq 2\pi i^{n-m}\frac{(m+n)!}{m!n!}\left(\frac{\tau_{\mathbf{q}\sigma}}{\hbar}\right)^{m+n+1}$$
$$\times \delta(\epsilon_{\mathbf{q}\sigma} - \epsilon) \qquad (C4)$$

to arrive at the following form for the in-plane conductivity components

$$\sigma^{ijj} = -\frac{4e^3}{\hbar}\text{Re}\sum_\mathbf{q}\left[\partial_\omega\mathcal{V}_{\mathbf{q}+}^i(\epsilon_F, \epsilon_F + \hbar\omega)|_{\omega=0}\right.$$
$$\left. + i\mathcal{V}_{\mathbf{q}+}^{iF}\tau_{\mathbf{q}+}^F\left(1 + i\frac{\partial\Gamma_{\mathbf{q}+}^F}{\partial\epsilon_F}\right)\right]v_{\mathbf{q}+}^j \mathcal{V}_{\mathbf{q}+}^{jF}(\tau_{\mathbf{q}+}^F)^2\delta(\epsilon_{\mathbf{q}+} - \epsilon_F), \qquad (C5)$$

where $\Gamma_{\mathbf{q}\sigma}^F$ and $\tau_{\mathbf{q}\sigma}^F$ are the self-energy and scattering time at the Fermi level. In this form, the quadratic conductivity tensor is expressed entirely in terms of the velocity vertex function and scattering time at the Fermi level, the former of which has, in general, been argued to play an important role in the nonlinear transport in Dirac systems [70,71]. Plots of the angular dependencies of these two quantities for various sweeps of the magnetization are presented in Fig. 4.
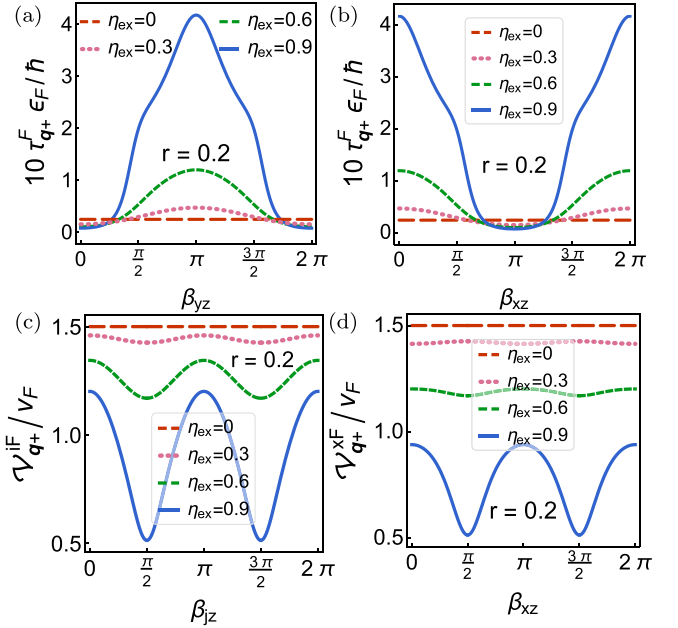

FIG. 4. Angular dependencies at the Fermi level. (a) Scattering time (with $q_y = 0$) in the yz plane; (b) ith component of the velocity vertex function (with $q_j = 0$) in the jz plane, where $i/j = x/y$ or y/x. (c) Scattering time (with $q_x = 0$) in the xz plane and (d) longitudinal velocity vertex function (with $q_y = 0$) in the xz plane. Parameters used: $\epsilon_F = 0.5$ eV, $v_F = 5 \times 10^{14}$ nm/s [58], and $\eta_I = 0.01$.

APPENDIX D: ANGULAR DEPENDENCIES WITH WEAK SOC DISORDER

Here, we analyze the angular dependencies of the UMR coefficients in the limit where the SOC disorder is weaker than
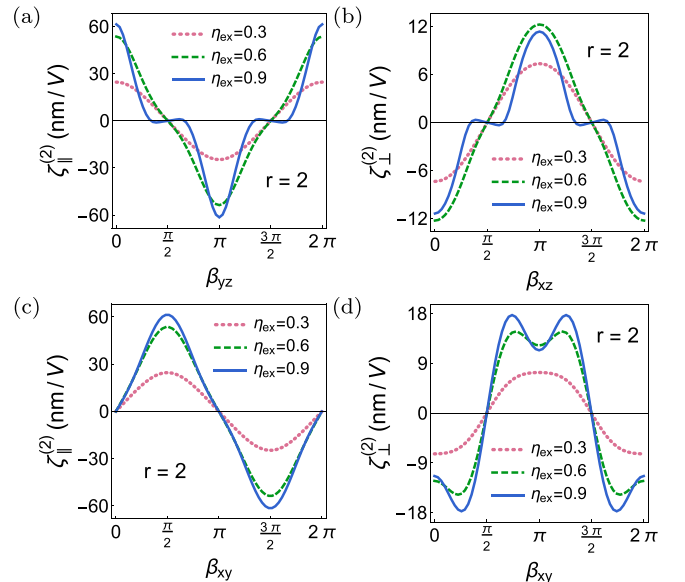

FIG. 5. Angular dependencies of the UMR coefficients for various angular sweeps of the magnetization. Here, β_{ij} ($i, j = x, y, z$) is the angle between the i axis and the magnetization as it sweeps the ij plane. Parameters used: $\epsilon_F = 0.5$ eV, $v_F = 5 \times 10^{14}$ nm/s [58], and $\eta_I = 0.01$.

the scalar disorder. We thus set $r = 2$ and plot the UMR coefficients, which are presented in Fig. 5. The first notable feature is that compared to the plots in Fig. 3—wherein $r = 0.2$—the amplitudes of the UMR and NPHE are generally weaker here for various in-plane and out-of-plane magnetization sweeps. This is not surprising, as the effects are generated in the presence of SOC disorder, which is also weaker here.

Another interesting feature is the qualitative behavior of the UMR coefficients when the Fermi level approaches the exchange energy. For out-of-plane sweeps of the magnetization, as shown in Figs. 5(a) and 5(b), for lower values of η_{ex} (see the dotted pink and dashed green curves), the UMR (NPHE) displays typical sinusoidal behavior, with two symmetry-imposed sign changes at $\beta_{yz}(\beta_{xz}) = \pi/2, 3\pi/2$. However, at

$\eta_{\mathrm{ex}} = 0.9$ (see the solid blue curves), four additional sign change points appear, which are connected by quasiplateaus of suppressed conductivity.

In order to gain further insight into the emergence of quasiplateaus and additional sign change points in the nonlinear magnetoresistances, it is convenient to obtain an approximate analytical expression for the conductivity tensor. As the irregularities in the angular dependencies emerge when the magnetization is almost out of plane, we may treat the in-plane components of the unit magnetization vector as perturbative parameters in the quasiplateau-forming angular region. Inserting Eqs. (B2) and (B3) into Eq. (C3), to first order in m_x and m_y, the dressed velocity vertex function may be expressed as

$$\boldsymbol{\mathcal{V}}_{\mathbf{q}\sigma}(\epsilon, \epsilon + \hbar\omega) = \mathcal{I}_\sigma(\boldsymbol{\eta_h}, \eta_{\mathrm{ex}}, m_z, \Gamma_\alpha, \Gamma_I; \omega)\mathbf{v}_{\mathbf{q}\sigma} + v_F\mathbf{z} \times [\mathcal{J}_\sigma(\boldsymbol{\eta_h}, \eta_{\mathrm{ex}}, m_z, \Gamma_\alpha, \Gamma_I; \omega)\boldsymbol{\eta_h} + \eta_{\mathrm{ex}}\mathcal{K}_\sigma(\boldsymbol{\eta_h}, \eta_{\mathrm{ex}}, m_z, \Gamma_\alpha, \Gamma_I; \omega)\mathbf{m}], \tag{D1}$$

where the dimensionless functions $\mathcal{I}_\sigma$, $\mathcal{J}_\sigma$, and $\mathcal{K}_\sigma$ are given by

$$\mathcal{I}_\sigma(\boldsymbol{\eta_h}, \eta_{\mathrm{ex}}, m_z, \Gamma_\alpha, \Gamma_I; \omega) = \frac{\Gamma_\alpha(1 - \eta_{\mathrm{ex}}^2 m_z^2)\big[9(1 - \eta_{\mathrm{ex}}^2 m_z^2) + \eta_\mathbf{h}^2\big] + \Gamma_I(3 + \eta_{\mathrm{ex}}^2 m_z^2) \mp i\hbar\omega}{8\Gamma_\alpha(1 - \eta_{\mathrm{ex}}^2 m_z^2)^2 + 2\Gamma_I(1 + \eta_{\mathrm{ex}}^2 m_z^2) \mp i\hbar\omega}, \tag{D2a}$$

$$\mathcal{J}_\sigma(\boldsymbol{\eta_h}, \eta_{\mathrm{ex}}, m_z, \Gamma_\alpha, \Gamma_I; \omega) = \frac{2\Gamma_\alpha(1 - \eta_{\mathrm{ex}}^2 m_z^2)(1 - \sigma\eta_{\mathrm{ex}}m_z\cos\theta_\mathbf{h})}{8\Gamma_\alpha(1 - \eta_{\mathrm{ex}}^2 m_z^2)^2 + 2\Gamma_I(1 + \eta_{\mathrm{ex}}^2 m_z^2) \mp i\hbar\omega}, \tag{D2b}$$

$$\begin{aligned}
\mathcal{K}_\sigma(\boldsymbol{\eta_h}, \eta_{\mathrm{ex}}, m_z, \Gamma_\alpha, \Gamma_I; \omega) = &-\frac{4\Gamma_\alpha(1 - \eta_{\mathrm{ex}}^2 m_z^2)}{\big[8\Gamma_\alpha(1 - \eta_{\mathrm{ex}}^2 m_z^2)^2 + 2\Gamma_I(1 + \eta_{\mathrm{ex}}^2 m_z^2) \mp i\hbar\omega\big]^2} \\
&\times \big\{4\Gamma_\alpha(1 - \eta_{\mathrm{ex}}^2 m_z^2)(1 - \eta_{\mathrm{ex}}^2 m_z^2 - \eta_\mathbf{h}^2)(1 - \sigma\eta_{\mathrm{ex}}m_z\cos\theta_\mathbf{h}) \\
&- 2\Gamma_I\big[1 - 3\eta_{\mathrm{ex}}^2 m_z^2 + \sigma\eta_{\mathrm{ex}}m_z(3 - \eta_{\mathrm{ex}}^2 m_z^2)\cos\theta_\mathbf{h} - \sigma\eta_\mathbf{h}(1 + \eta_{\mathrm{ex}}^2 m_z^2)\sin\theta_\mathbf{h}\big] \\
&\mp i\hbar\omega[1 - \sigma\eta_{\mathrm{ex}}m_z\cos\theta_\mathbf{h} + \sigma\eta_\mathbf{h}\sin\theta_\mathbf{h}]\big\}. \tag{D2c}
\end{aligned}$$

Inserting this solution into Eq. (C5), the longitudinal and transverse conductivities read

$$\sigma_{xxx} = -\frac{9e^3 v_F}{32\pi\epsilon_F^2}m_y\,\mathcal{C}(\eta_\alpha, \eta_I, \eta_{\mathrm{ex}}, m_z), \tag{D3a}$$

$$\sigma_{yxx} = \frac{3e^3 v_F}{32\pi\epsilon_F^2}m_x\,\mathcal{C}(\eta_\alpha, \eta_I, \eta_{\mathrm{ex}}, m_z), \tag{D3b}$$

where η_{ex} is understood to be calculated at the Fermi level and the dimensionless function $\mathcal{C}$ is given by

$$\begin{aligned}
\mathcal{C}(\eta_\alpha, \eta_I, \eta_{\mathrm{ex}}, m_z) = &\,\eta_\alpha\eta_{\mathrm{ex}}(1 - \eta_{\mathrm{ex}}^2 m_z^2)^2\big[12\eta_\alpha(1 - \eta_{\mathrm{ex}}^2 m_z^2)^2 + \eta_I(1 - 3\eta_{\mathrm{ex}}^2 m_z^2)\big] \\
&\times \big[12\eta_\alpha(1 - \eta_{\mathrm{ex}}^2 m_z^2)^2 + \eta_I(3 + \eta_{\mathrm{ex}}^2 m_z^2)\big]^2\big[4\eta_\alpha(1 - \eta_{\mathrm{ex}}^2 m_z^2)^2 + \eta_I(1 + \eta_{\mathrm{ex}}^2 m_z^2)\big]^{-6}, \tag{D4}
\end{aligned}$$

leading to the UMR coefficients

$$\zeta_\parallel^{(2)} = \frac{9e^3 v_F}{16\pi\sigma_D\epsilon_F^2}m_y\,\mathcal{C}(\eta_\alpha, \eta_I, \eta_{\mathrm{ex}}, m_z), \tag{D5a}$$

$$\zeta_\perp^{(2)} = -\frac{3e^3 v_F}{16\pi\sigma_D\epsilon_F^2}m_x\,\mathcal{C}(\eta_\alpha, \eta_I, \eta_{\mathrm{ex}}, m_z). \tag{D5b}$$

Note that in this approximation, the ratio between the longitudinal and transverse UMR coefficients takes the simple

form

$$\frac{\zeta_\perp^{(2)}}{\zeta_\parallel^{(2)}} = -\frac{1}{3}\cot\phi_\mathbf{m}, \tag{D6}$$

where $\phi_\mathbf{m}$ is the angle between the electric field and magnetization, further confirming the common physical origin of the two nonlinear magnetoresistances.

Figures 5(a) and 5(b) reveal that when an out-of-plane angular sweep of the magnetization is performed, there will be a total of six angles where the longitudinal or transverse UMR
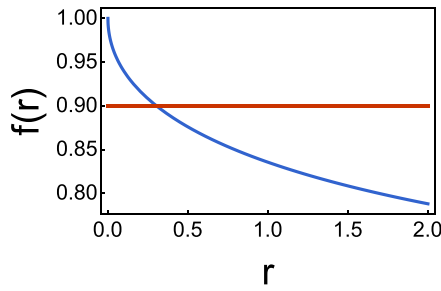
FIG. 6. Plot of the monotonically decreasing function $f(r)$ (blue), with the red horizontal line indicating the value of $\eta_{ex} = 0.9$ for comparison. The unconventional angular dependencies of the conductivities emerge when $\eta_{ex} > f(r)$.

coefficients vanish. Two of these are the conventional angles where the in-plane magnetization vanishes ($\beta_{yz} = \pi/2, 3\pi/2$ for the UMR and $\beta_{xz} = \pi/2, 3\pi/2$ for the NPHE). The other four must than correspond to solutions of $\mathcal{C} = 0$, which turn out to be $\beta_{yz} = \pi/2 \pm \theta_p/2, 3\pi/2 \pm \theta_p/2$, and similarly for β_{xz}, where θ_p is the angular arc over which the conductivities display a plateaulike profile and is given by $\theta_p = 2\cos^{-1}[f(r)/\eta_{ex}]$, where $r = \eta_I/\eta_\alpha$ and the dimensionless

function $f(r)$ is

$$f(r) = \sqrt{1 + \frac{r}{8}\left(1 - \sqrt{1 + \frac{32}{3r}}\right)}. \tag{D7}$$

For the parameters used in obtaining Figs. 5(a) and 5(b), $\eta_{ex} = 0.9$ and $r = 2$, we find that $\theta_p \approx \pi/3$, which is quite sizable. From Eq. (D7), we may deduce the requirement the system imposes for the additional sign changes of the nonlinear conductivity—and therefore the emergence of the quasiplateaus—to occur. From the condition that $\theta_p > 0$, we conclude that the system must satisfy $\eta_{ex} > f(r)$. This requirement—or its lack thereof—is met by all the curves in Figs. 3(a) and 3(c), as well as the ones presented in Fig. 5, further confirming the validity of the analytical approximation. In addition, as displayed in Fig. 6, $f(r)$ is a monotonically decreasing function. From this fact, and the requirement that $\eta_{ex} > f(r)$, we conclude that in order for the system to allow for additional sign changes of the nonlinear magnetoresistances and the subsequent emergence of plateaulike profiles, the Fermi level must be sufficiently close to the exchange energy and the density of the scalar scatterers must be sufficiently higher than that of the SOC impurities.

[1] K. N. Okada, N. Ogawa, R. Yoshimi, A. Tsukazaki, K. S. Takahashi, M. Kawasaki, and Y. Tokura, Phys. Rev. B **93**, 081403(R) (2016).

[2] K. Kondou, R. Yoshimi, A. Tsukazaki, Y. Fukuma, J. Matsuno, K. S. Takahashi, M. Kawasaki, Y. Tokura, and Y. Otani, Nat. Phys. **12**, 1027 (2016).

[3] R. Sun, S. Yang, X. Yang, E. Vetter, D. Sun, N. Li, L. Su, Y. Li, Y. Li, Z.-z. Gong et al., Nano Lett. **19**, 4420 (2019).

[4] S. H. Su, P.-Y. Chuang, J.-C. Lee, C.-W. Chong, Y. W. Li, Z. M. Lin, Y.-C. Chen, C.-M. Cheng, and J.-C.-A. Huang, ACS Appl. Electron. Mater. **3**, 2988 (2021).

[5] X.-L. Qi, Y.-S. Wu, and S.-C. Zhang, Phys. Rev. B **74**, 085308 (2006).

[6] R. Yu, W. Zhang, H.-J. Zhang, S.-C. Zhang, X. Dai, and Z. Fang, Science **329**, 61 (2010).

[7] C.-Z. Chang, J. Zhang, X. Feng, J. Shen, Z. Zhang, M. Guo, K. Li, Y. Ou, P. Wei, L.-L. Wang et al., Science **340**, 167 (2013).

[8] J. Checkelsky, R. Yoshimi, A. Tsukazaki, K. Takahashi, Y. Kozuka, J. Falson, M. Kawasaki, and Y. Tokura, Nat. Phys. **10**, 731 (2014).

[9] C.-X. Liu, S.-C. Zhang, and X.-L. Qi, Annu. Rev. Condens. Matter Phys. **7**, 301 (2016).

[10] C.-Z. Chang, C.-X. Liu, and A. H. MacDonald, Rev. Mod. Phys. **95**, 011002 (2023).

[11] H. Wu, F. Groß, B. Dai, D. Lujan, S. A. Razavi, P. Zhang, Y. Liu, K. Sobotkiewich, J. Förster, M. Weigand et al., Adv. Mater. **32**, 2003380 (2020).

[12] P. Li, J. Ding, S. S.-L. Zhang, J. Kally, T. Pillsbury, O. G. Heinonen, G. Rimal, C. Bi, A. DeMann, S. B. Field et al., Nano Lett. **21**, 84 (2021).

[13] X. Zhang, S. C. Ambhire, Q. Lu, W. Niu, J. Cook, J. S. Jiang, D. Hong, L. Alahmed, L. He, R. Zhang et al., ACS Nano **15**, 15710 (2021).

[14] A. R. Mellnik, J. S. Lee, A. Richardella, J. L. Grab, P. J. Mintun, M. H. Fischer, A. Vaezi, A. Manchon, E.-A. Kim, N. Samarth et al., Nature (London) **511**, 449 (2014).

[15] J. Han, A. Richardella, S. A. Siddiqui, J. Finley, N. Samarth, and L. Liu, Phys. Rev. Lett. **119**, 077702 (2017).

[16] P. Li, J. Kally, S. S.-L. Zhang, T. Pillsbury, J. Ding, G. Csaba, J. Ding, J. Jiang, Y. Liu, R. Sinclair et al., Sci. Adv. **5**, eaaw3415 (2019).

[17] A. G. Moghaddam, A. Qaiumzadeh, A. Dyrdał, and J. Berakdar, Phys. Rev. Lett. **125**, 196801 (2020).

[18] T. Chiba, S. Takahashi, and G. E. W. Bauer, Phys. Rev. B **95**, 094428 (2017).

[19] J. Sklenar, Y. Zhang, M. B. Jungfleisch, Y. Kim, Y. Xiao, G. J. MacDougall, M. J. Gilbert, A. Hoffmann, P. Schiffer, and N. Mason, Appl. Phys. Lett. **118**, 232402 (2021).

[20] H. Wu, A. Chen, P. Zhang, H. He, J. Nance, C. Guo, J. Sasaki, T. Shirokura, P. N. Hai, B. Fang et al., Nat. Commun. **12**, 6251 (2021).

[21] L. Fu and C. L. Kane, Phys. Rev. Lett. **100**, 096407 (2008).

[22] B. Lian, X.-Q. Sun, A. Vaezi, X.-L. Qi, and S.-C. Zhang, Proc. Natl. Acad. Sci. **115**, 10938 (2018).

[23] K. Yasuda, A. Tsukazaki, R. Yoshimi, K. S. Takahashi, M. Kawasaki, and Y. Tokura, Phys. Rev. Lett. **117**, 127202 (2016).

[24] K. Yasuda, A. Tsukazaki, R. Yoshimi, K. Kondou, K. S. Takahashi, Y. Otani, M. Kawasaki, and Y. Tokura, Phys. Rev. Lett. **119**, 137204 (2017).

[25] Y. Lv, J. Kally, D. Zhang, J. S. Lee, M. Jamali, N. Samarth, and J.-P. Wang, Nat. Commun. **9**, 1 (2018).

[26] N. H. Duy Khang and P. N. Hai, J. Appl. Phys. **126**, 233903 (2019).

[27] Y. Wang, S. V. Mambakkam, Y.-X. Huang, Y. Wang, Y. Ji, C. Xiao, S. A. Yang, S. A. Law, and J. Q. Xiao, Phys. Rev. B **106**, 155408 (2022).

[28] Y. Lv, J. Kally, T. Liu, P. Quarterman, T. Pillsbury, B. J. Kirby, A. J. Grutter, P. Sahu, J. A. Borchers, M. Wu *et al.*, Appl. Phys. Rev. **9**, 011406 (2022).

[29] C. O. Avci, K. Garello, A. Ghosh, M. Gabureac, S. F. Alvarado, and P. Gambardella, Nat. Phys. **11**, 570 (2015).

[30] K. Olejník, V. Novák, J. Wunderlich, and T. Jungwirth, Phys. Rev. B **91**, 180402(R) (2015).

[31] S. S.-L. Zhang and G. Vignale, Phys. Rev. B **94**, 140411(R) (2016).

[32] T. Guillet, A. Marty, C. Vergnaud, M. Jamet, C. Zucchetti, G. Isella, Q. Barbedienne, H. Jaffrès, N. Reyren, J. M. George *et al.*, Phys. Rev. B **103**, 064411 (2021).

[33] J. Železný, Z. Fang, K. Olejník, J. Patchett, F. Gerhard, C. Gould, L. W. Molenkamp, C. Gomez-Olivella, J. Zemen, T. Tichý *et al.*, Phys. Rev. B **104**, 054429 (2021).

[34] X. Zhou, F. Zeng, M. Jia, H. Chen, and Y. Wu, Phys. Rev. B **104**, 184413 (2021).

[35] G. Liu, X.-G. Wang, Z. Z. Luan, L. F. Zhou, S. Y. Xia, B. Yang, Y. Z. Tian, G.-h. Guo, J. Du, and D. Wu, Phys. Rev. Lett. **127**, 207206 (2021).

[36] T. H. T. Nguyen, V. Q. Nguyen, S. Jeong, E. Park, H. Jang, N. J. Lee, S. Lee, B.-G. Park, S. Cho, H.-W. Lee *et al.*, Commun. Phys. **4**, 247 (2021).

[37] K. Hasegawa, T. Koyama, and D. Chiba, Phys. Rev. B **103**, L020411 (2021).

[38] M. Mehraeen and S. S.-L. Zhang, Phys. Rev. B **105**, 184423 (2022).

[39] S. Shim, M. Mehraeen, J. Sklenar, J. Oh, J. Gibbons, H. Saglam, A. Hoffmann, S. S.-L. Zhang, and N. Mason, Phys. Rev. X **12**, 021069 (2022).

[40] K. Lou, Q. Zhao, B. Jiang, and C. Bi, Phys. Rev. Appl. **17**, 064052 (2022).

[41] S. Ding, P. Noël, G. K. Krishnaswamy, and P. Gambardella, Phys. Rev. Res. **4**, L032041 (2022).

[42] Y. Fan, P. Zhang, J. Han, Y. Lv, L. Liu, and J.-P. Wang, Adv. Electron. Mater. **9**, 2300232 (2023).

[43] Y. Cheng, J. Tang, J. J. Michel, S. K. Chong, F. Yang, R. Cheng, and K. L. Wang, Phys. Rev. Lett. **130**, 086703 (2023).

[44] S. Wang, X. Cui, R. Xie, C. Zhang, Y. Tian, L. Bai, Q. Huang, Q. Cao, and S. Yan, Phys. Rev. B **107**, 094410 (2023).

[45] Z. Zheng, Y. Gu, Z. Zhang, X. Zhang, T. Zhao, H. Li, L. Ren, L. Jia, R. Xiao, H.-A. Zhou *et al.*, Nano Lett. **23**, 6378 (2023).

[46] M. Mehraeen, P. Shen, and S. S.-L. Zhang, Phys. Rev. B **108**, 014411 (2023).

[47] It should be stressed that the SOC disorder is a required element, as without it, the in-plane magnetization–a key UMR ingredient–can be gauged out of the problem [18,52].

[48] E. Y. Sherman, Phys. Rev. B **67**, 161303(R) (2003).

[49] L. E. Golub and E. L. Ivchenko, Phys. Rev. B **69**, 115333 (2004).

[50] A. Ström, H. Johannesson, and G. I. Japaridze, Phys. Rev. Lett. **104**, 256804 (2010).

[51] L. Kimme, B. Rosenow, and A. Brataas, Phys. Rev. B **93**, 081301(R) (2016).

[52] A. Dyrdał, J. Barnaś, and A. Fert, Phys. Rev. Lett. **124**, 046802 (2020).

[53] V. K. Dugaev, M. Inglot, E. Ya. Sherman, J. Berakdar, and J. Barnaś, Phys. Rev. Lett. **109**, 206601 (2012).

[54] R. Kubo, J. Phys. Soc. Jpn. **12**, 570 (1957).

[55] D. E. Parker, T. Morimoto, J. Orenstein, and J. E. Moore, Phys. Rev. B **99**, 045121 (2019).

[56] Z. Du, C. Wang, H.-P. Sun, H.-Z. Lu, and X. Xie, Nat. Commun. **12**, 1 (2021).

[57] H. Rostami, M. I. Katsnelson, G. Vignale, and M. Polini, Ann. Phys. **431**, 168523 (2021).

[58] X.-L. Qi and S.-C. Zhang, Rev. Mod. Phys. **83**, 1057 (2011).

[59] It is worth noting that these angular dependence trends of the NPHE for both out-of-plane and in-plane sweeps of the magnetization resemble the behavior predicted for the planar Hall effect in the linear response regime [18].

[60] P. He, S. S.-L. Zhang, D. Zhu, Y. Liu, Y. Wang, J. Yu, G. Vignale, and H. Yang, Nat. Phys. **14**, 495 (2018).

[61] P. He, S. S.-L. Zhang, D. Zhu, S. Shi, O. G. Heinonen, G. Vignale, and H. Yang, Phys. Rev. Lett. **123**, 016801 (2019).

[62] S. Langenfeld, V. Tshitoyan, Z. Fang, A. Wells, T. Moore, and A. Ferguson, Appl. Phys. Lett. **108**, 192402 (2016).

[63] W. P. Sterk, D. Peerlings, and R. A. Duine, Phys. Rev. B **99**, 064438 (2019).

[64] I. Sodemann and L. Fu, Phys. Rev. Lett. **115**, 216806 (2015).

[65] D. Zhang, M. Shi, T. Zhu, D. Xing, H. Zhang, and J. Wang, Phys. Rev. Lett. **122**, 206401 (2019).

[66] H. Wang, D. Wang, Z. Yang, M. Shi, J. Ruan, D. Xing, J. Wang, and H. Zhang, Phys. Rev. B **101**, 081109(R) (2020).

[67] Q. Liu, C.-X. Liu, C. Xu, X.-L. Qi, and S.-C. Zhang, Phys. Rev. Lett. **102**, 156603 (2009).

[68] D. A. Abanin and D. A. Pesin, Phys. Rev. Lett. **106**, 136802 (2011).

[69] K. Nomura and N. Nagaosa, Phys. Rev. Lett. **106**, 166802 (2011).

[70] H. Rostami and E. Cappelluti, Phys. Rev. B **103**, 125415 (2021).

[71] H. Rostami and E. Cappelluti, npj 2D Mater. Appl. **5**, 50 (2021).